Volume 1
Number 1
March 2024
Pages 1–146

RSC Mechanochemistry

rsc.li/RSCMechanochem

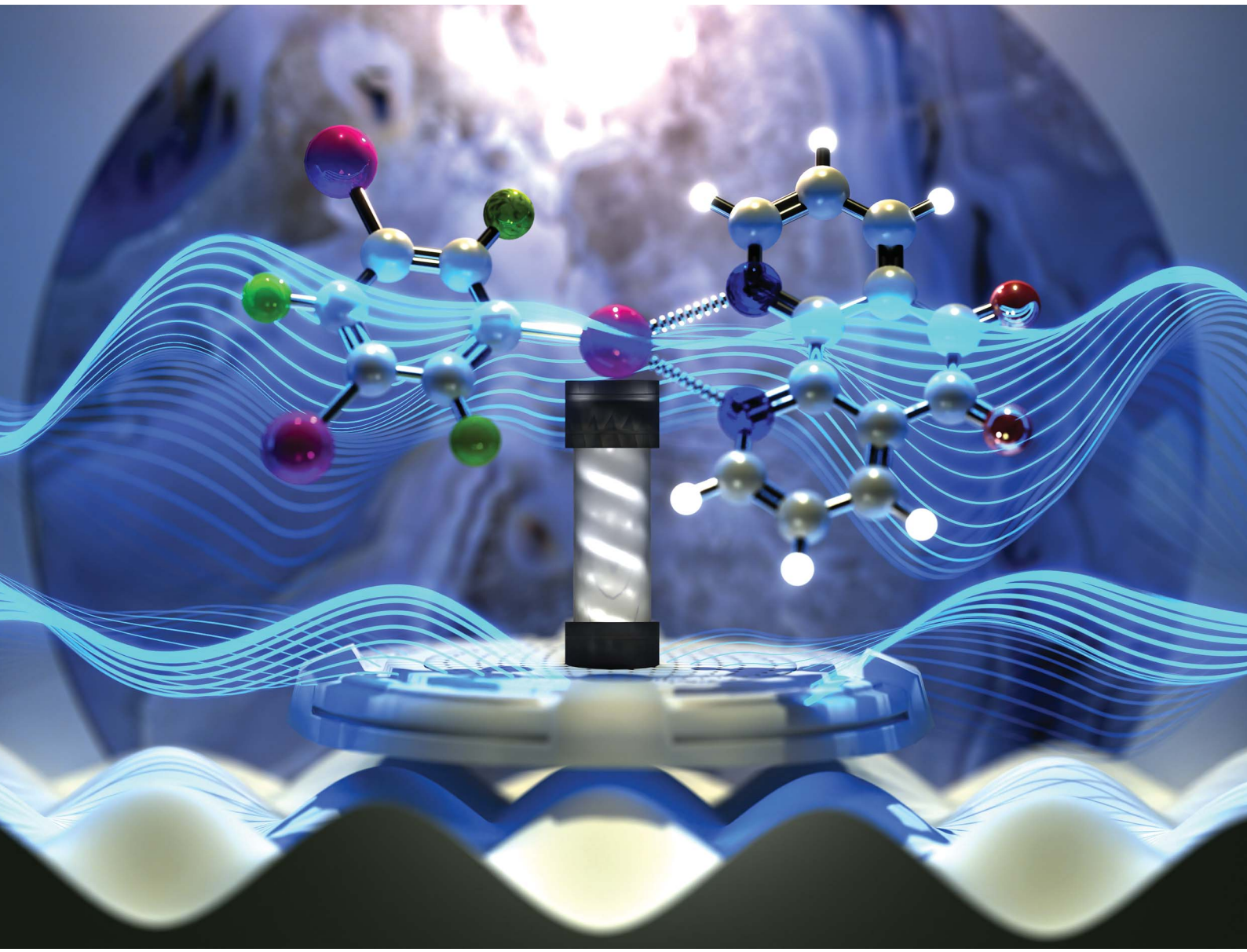

ISSN 2976-8683

ROYAL SOCIETY OF CHEMISTRY

PAPER
David L. Bryce *et al.*
Halogen-bonded cocrystals *via* resonant acoustic mixing

RSC Mechanochemistry

ROYAL SOCIETY OF CHEMISTRY

PAPER

View Article Online
View Journal | View Issue

Cite this: *RSC Mechanochem.*, 2024, **1**, 50

Halogen-bonded cocrystals *via* resonant acoustic mixing†

Alireza Nari, Jeffrey S. Ovens and David L. Bryce *

Resonant acoustic mixing is a relatively gentle mechanochemical technology that employs pressure waves to induce chemical and morphological transformations. We report here on the production of eleven halogen-bonded (XB) cocrystalline architectures *via* neat and liquid-assisted resonant acoustic mixing (RAM). Two strong iodinated XB donors, namely 1,4-diiodotetrafluorobenzene (*p*-DITFB, **1**) and 1,3,5-trifluoro-2,4,6-triiodobenzene (*sym*-TFTIB, **2**) each react with five XB donors, namely 2,3,5,6-tetramethylpyrazine (TMP, **a**), 4-dimethylaminopyridine (DMAP, **b**), 1,10-phenanthroline (*o*-Ph, **c**), 1,10-phenanthroline-5,6-dione (PheDON, **d**), and 4,5-diazafluoren-9-one (DIZFON, **e**) to form ten cocrystals. For these systems, it is shown that RAM is capable of producing the same products as are obtained *via* ball milling. Two novel cocrystals are obtained (of **2d** featuring bifurcated XBs, and **2e** featuring monofurcated XBs) and their single-crystal X-ray structures are reported. However, an eleventh stoichiomorphic cocrystal of *p*-DITFB and TMP is obtained exclusively *via* RAM, suggesting that the combination of RAM and milling approaches may afford a broader exploration of the polymorphic and stoichiomorphic landscape than the use of a single technique in isolation. All products are characterized *via* powder X-ray diffraction, and ^{13}C cross-polarization magic angle spinning (CP/MAS) and ^{19}F MAS NMR spectroscopy, providing further evidence for the phase purity of samples obtained from RAM experiments and for the degree of polymorphic control available when small volumes of liquid are employed in mechanochemical reactions. This work demonstrates the potential of RAM for the production of known and novel halogen-bonded cocrystalline assemblies, including polymorphic and stoichiomorphic structures.

Received 8th December 2023
Accepted 16th January 2024

DOI: 10.1039/d3mr00028a

rsc.li/RSCMechanochem

Introduction

Halogen bonding (XB), a distinctive noncovalent interaction, has surged in interest due to its directional and tunable characteristics,[1,2] enabling the deliberate design of frameworks[3,4] and control of biomolecular structure.[5,6] This interaction involves the electrophilic region of a covalently bonded halogen (termed the σ-hole)[7] on the halogen bond donor engaging with a Lewis base as the halogen bond acceptor.[8] The presence of this interaction is often assessed using the normalized contact distance ratio, R_{XB},[9] which gauges the halogen bond distance ($d_{X\cdots Y}$) relative to the sum of the van der Waals radii of the atoms involved ($\sum d_{vdw}$):[10]

$$R_{XB} = \frac{d_{X\cdots Y}}{\sum d_{vdw}}.$$

Over the past two decades, halogen bonding has emerged as a versatile tool, finding applications across diverse domains such as crystal engineering, medicinal chemistry,[11,12] anion recognition,[13,14] supramolecular systems,[15] and catalysis.[16,17] Its adaptable nature and the potential for precise modulation make halogen bonding an intriguing avenue for innovative molecular design and tailored interactions.

Mechanochemistry, a dynamic and evolving field, has emerged as an innovative approach to chemical synthesis and materials discovery. This methodology harnesses mechanical force, such as grinding or milling, as a key driver in chemical reactions, replacing or complementing traditional solution-based processes.[18,19] The concept of mechanochemistry dates back to the 19th century when it was first noted that certain reactions occurred more readily under mechanical action.[20–22] However, it wasn't until recent decades that the full potential of mechanochemistry began to be realized. Today, this field offers a versatile platform for green and sustainable chemistry,[23,24] with applications ranging from pharmaceuticals[25–27] to catalysis,[28–33] and materials science.[34,35]

Department of Chemistry and Biomolecular Sciences, Centre for Catalysis Research and Innovation, and Nexus for Quantum Technologies, University of Ottawa, Ottawa, Ontario, Canada K1N6N5. E-mail: dbryce@uottawa.ca; Fax: +1-613-562-5170; Tel: +1-613-562-5800

† Electronic supplementary information (ESI) available: Further synthetic details; additional NMR spectra; powder X-ray diffractograms. Crystallographic information files for compounds **2d** and **2e** have been deposited with the CCDC with cif numbers 2305189 and 2305188. For ESI and crystallographic data in CIF or other electronic format see DOI: https://doi.org/10.1039/d3mr00028a

In addition to the absence of solvents offering advantages, solid-state reactions frequently yield highly pure products and can be conducted using uncomplicated equipment, such as basic manual grinding[36] or mechanical milling.[37–39] Occasionally, a small quantity of liquid is introduced into mechanochemical reactions to expedite the transformation or facilitate the reaction, which, in certain instances, may induce polymorphic variations.[40] These reactions can be categorized as "minimal solvent" rather than purely "solvent-free",[18] and they are often referred to as kneading, solvent drop grinding, or, in a more comprehensive and contemporary context, liquid-assisted grinding (LAG).[41,42]

Mechanochemical reactions are often characterized by their unique ability to access reaction pathways and product formations that are often elusive through traditional methods.[43] The fundamental principles behind mechanochemistry involve the application of mechanical energy to overcome activation barriers and promote bond cleavage, facilitating the synthesis of complex molecules and materials. As a result, mechanochemistry has garnered increasing interest within the scientific community for its potential to revolutionize the way we approach chemical synthesis and discover new materials. Recent advances in the field have demonstrated its efficacy in preparing cocrystals,[44–49] polymorphs,[50] and metal–organic frameworks,[51,52] highlighting its versatility and potential in various applications.

Here, we provide a proof of principle study of direct mechanochemical halogen bond-induced cocrystallization by resonant acoustic mixing (RAM), focusing on the reduction of reaction time and the engineering of cocrystals featuring I···N and I···O interactions (Fig. 1). We show that acoustic mechanochemistry with RAM, leveraging acoustic wave pressure as the driving force, can efficiently provide the energy required for promoting halogen bond-induced cocrystallization. Cocrystal synthesis *via* RAM has been reported previously,[53–58] but to our knowledge the production of halogen-bonded systems has not been systematically explored.

Furthermore, our ongoing work focuses on fine-tuning the coordination of XB interactions using RAM methodology. Notably, in a recent study by Michalczyk *et al.*,[59] it was reported that only 2% of XB cocrystals exhibit bifurcated interactions, underscoring the rarity of such configurations obtained *via* traditional methods. The efficiency of RAM in forging XB interactions may hold the potential to unlock bifurcated and multi-coordinated XB interactions, thus broadening the possibilities for tailoring cocrystals in ways that were previously inaccessible through traditional mechanochemical approaches.

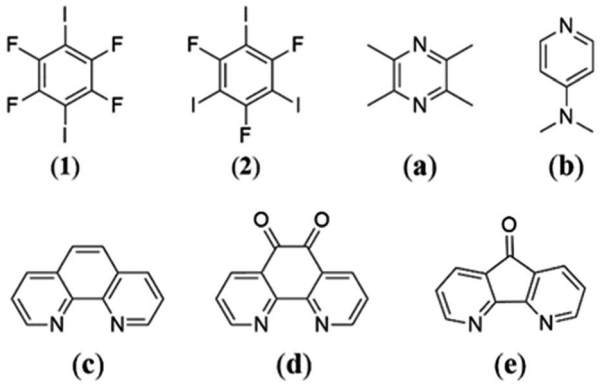

Cocrystals Obtained:

4(p-DITFB).1.5(TMP): **1a(ii)**	(p-DITFB).2(TMP): **1a(i)**
(p-DITFB).2(DMAP): **1b**	(sym-TFTIB).(TMP): **2a**
2(p-DITFB).(o-Phe): **1c**	(sym-TFTIB).3(DMAP): **2b**
(p-DITFB).(PheDON): **1d**	(sym-TFTIB).(o-Phe): **2c**
(p-DITFB).(DIZFON): **1e**	(sym-TFTIB).(PheDON): **2d**
	(sym-TFTIB).(DIZFON): **2e**

Fig. 1 Molecular structure of halogen bond donors and acceptors studied herein with the cocrystals obtained.

Experimental section

(i) General

1,4-Diiodotetrafluorobenzene (*p*-DITFB, **1**), 2,3,5,6-tetramethylpyrazine (TMP, **a**), and 4-dimethylaminopyridine (DMAP, **b**), were purchased from Sigma-Aldrich. 1,10-Phenanthroline (*o*-Ph, **c**) and 1,10-phenanthroline-5,6-dione (PheDON, **d**) were purchased from Fisher Scientific. 4,5-Diazafluoren-9-one (DIZFON, **e**) was purchased from TCI. 1,3,5-Trifluoro-2,4,6-triiodobenzene (*sym*-TFTIB, **2**) was purchased from SynQuest Laboratories. These compounds were utilized in their as-received state without further purification. Reagent grade solvents and doubly distilled water were used.

(ii) Mechanochemistry and sample preparation

Mechanochemical transformations were performed using ball milling (Retsch MM 400) and resonant acoustic mixing (Resodyn PharmaRAM 1) devices.

Ball milling. The production of each cocrystal was upscaled to generate 300 to 400 mg of the intended product. Both the halogen bond donor and the halogen bond acceptor at the indicated ratios were introduced into a 10 mL stainless steel milling jar. For cocrystallization using liquid assisted grinding (LAG), a small quantity (ranging from 0.1 to 0.5 μL mg^{-1}) of chloroform, acetonitrile, tetrahydrofuran, or methanol was added. The ball milling procedure was carried out at room temperature with a milling frequency of 30 Hz, spanning a duration of 30 to 45 min. This process utilized two stainless steel grinding balls, each with a diameter of 5 mm. The specific synthesis conditions for each cocrystal *via* ball milling are outlined in Table 1 and detailed procedures are explained in the ESI.†

Resonant acoustic mixing. In a standard procedure, specific amounts of finely powdered halogen bond donor and halogen bond acceptor were transferred into a 1-dram glass vial, securely mounted within a lab-built sample holder, and positioned on the RAM platform. To this reactant mixture, a liquid additive such as tetrahydrofuran, chloroform, or methanol was added within the range of 0 to 1.0 μL mg^{-1}. The blend was mixed vigorously using the PharmaRAM 1 instrument for a duration of 45 to 50 min, employing an acceleration of 80 *g* (*g*: acceleration of gravity). The

Table 1 Experimental synthesis conditions of cocrystals in this work

			Ball milling			RAM			
Compound	Molar ratio (donor : acceptor)	Masses (donor : acceptor) (mg)	Time (min)	Liquid	η (μL mg^{-1})	Time (min)	Liquid	η (μL mg^{-1})	Refcode
1a(i)	(1 : 1)	(241 : 82)	45	$CHCl_3$	0.10	50	$CHCl_3$	0.20	JAQMAQ[60]
1a(ii)	(2 : 1)	(402 : 68)	*NA*[a]	*NA*	*NA*	45	None	—	KIHRAX[61]
1b	(1 : 2)	(321 : 196)	45	None	—	45	None	—	RUYHID[62]
1c	(1 : 1)	(241 : 108)	45	$CHCl_3$	0.05	50	$CHCl_3$	0.10	JAQMIY[60]
1d	(1 : 1)	(205 : 105)	30	$CHCl_3$	0.10	50	THF	0.5	EXIFEX[63]
1e	(1 : 1)	(205 : 91)	30	$CHCl_3$	0.10	50	THF	0.5	EXIFAT[63]
2a	(1 : 1)	(357 : 95)	30	THF	0.05	50	THF	0.1	SAJCUE[9]
2b	(1 : 3)	(255 : 183)	45	None	—	50	None	—	RUYJAX[64]
2c	(1 : 1)	(255 : 90)	45	$CHCl_3$	0.05	50	THF	0.10	SAJDEP[9]
2d	(1 : 1)	(255 : 105)	45	$CHCl_3$	0.05	50	$CHCl_3$	0.7	This work
2e	(1 : 1)	(255 : 94)	45	$CHCl_3$	0.10	50	$CHCl_3$	0.7	This work

[a] Not achievable.

specific RAM synthesis conditions for each cocrystal are outlined in Table 1 and detailed procedures are explained in the ESI.†

Slow evaporation. To grow cocrystals of **2d** and **2e** suitable for single crystal X-ray diffraction (SCXRD), a solution of *sym*-TFTIB (0.15 mmol) dissolved in 2 mL of chloroform was added dropwise to a solution of PheDON or DIZON (0.15 mmol) also dissolved in 2 mL of chloroform. The solvent was allowed to gradually evaporate at room temperature, resulting in the formation of yellow and orange cocrystals for **2d** and **2e**, respectively, over the course of one week. Vials were tightly sealed as soon as single cocrystals were observed by eye.

(iii) Powder X-ray diffraction

Powder X-ray diffraction (PXRD) data were collected using a Bruker D8 Endeavor instrument that features a 1 kW Cu Kα radiation source from a sealed tube and a LynxEye XE-T high-speed detector operating at a wavelength of $\lambda = 1.54056$ Å. These measurements were conducted under standard room temperature conditions. The samples were securely positioned within a well plate and underwent a rotational motion at 15 revolutions per minute throughout the data collection process.

(iv) Single-crystal X-ray diffraction

Single cocrystals of compounds **2d** and **2e** were affixed onto a thin glass fiber using parabar oil. SCXRD analysis was conducted employing a Bruker AXS SMART single crystal diffractometer equipped with a sealed Mo tube source emitting radiation at a wavelength of 0.71073 Å. This analysis was carried out at a temperature of 213 K.

The diffraction dataset revealed systematic absences, and the unit cell parameters were in accordance with the monoclinic $P2_1/c$ crystal system for both compounds **2d** and **2e**. See ESI† for further details.

(v) Solid-state NMR spectroscopy

$^1H \rightarrow {}^{13}C$ cross-polarization magic-angle spinning (CPMAS) SSNMR experiments were conducted using a Bruker Avance III spectrometer operating at 9.4 T. A Bruker 4 mm HXY MAS probe was employed, and the spinning frequency was typically set to 11 kHz (see ESI† for further details). The CPMAS technique involved a 6 to 8 ms contact time, a proton $\pi/2$ pulse duration of 3.60 μs, and ^1H decoupling at a nutation frequency of 54.3 kHz. To determine chemical shifts, referencing was done relative to glycine at 176.4 ppm ($^{13}C=O$) with respect to TMS.

^{19}F MAS SSNMR experiments were conducted at 11.7 T, utilizing a Bruker Avance III spectrometer. For these experiments, a Bruker 2.5 mm HX MAS probe was employed, with a spinning frequency set at 25 kHz. The data acquisition employed a Bloch decay sequence with a $\pi/2$ pulse duration of 1.75 μs and a recycle delay of 60–90 seconds. Chemical shifts are reported with respect to polytetrafluoroethylene at −122.2 ppm.

Results and discussion

(i) Mechanochemistry and PXRD

The preparation of XB cocrystals can typically be achieved through both solution crystal growth and solid-state mechanochemistry. Nevertheless, mechanochemistry offers a rapid and efficient means of cocrystal synthesis while minimizing solvent usage and by-product formation. However, for obtaining molecular structural information and geometry, the use of single crystals is indispensable, which can be achieved through solvent-based crystallization. Herein, the employed cocrystallization techniques encompass neat solid-state and liquid-assisted ball milling and RAM. Additionally, solution growth methods were employed to produce single cocrystals of two novel compounds, *i.e.*, *sym*-TFTIB with PheDON and DIZFON (cocrystals **2d** and **2e**).

We describe here the mechanochemical preparation, *via* ball milling and RAM, of cocrystals **1a**, **2a**, **1b**, **2b**, **1c**, **2c**, **1d**, **2d**, **1e**, and **2e** (Fig. 1). Except for two novel cocrystals (**2d** and **2e**), the rest of these compounds had previously been cocrystallized through solution growth and characterized *via* SCXRD. This work therefore focusses on minimizing solvent usage and on exploring the potential of environmentally friendly and low energy consumption RAM mechanochemical methods for producing halogen-bonded compounds.

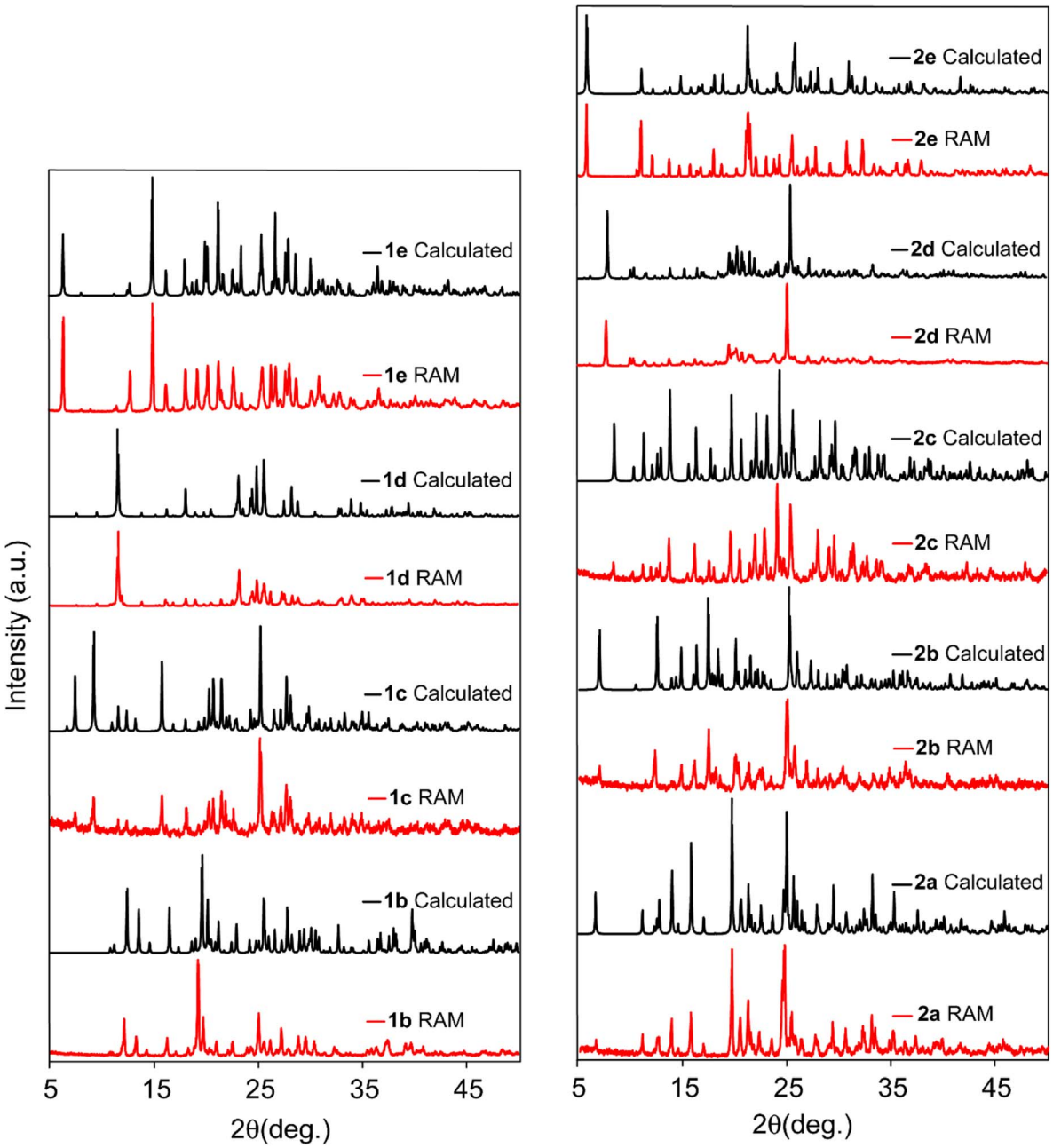

Fig. 2 Comparison between experimental PXRD patterns of cocrystals prepared *via* RAM (red) and the simulated X-ray powder patterns (black).

In all cases, the PXRD patterns depicted in Fig. 2 and in the ESI† reveal a notable similarity between the products obtained through ball milling and RAM methods when the same stoichiometry of reactants and identical synthesis conditions (*e.g.*, reaction time and liquid additive) were applied. Pure and stable forms of these cocrystals were obtained using RAM, typically within less than an hour (in most cases, around 40 min), under both neat and LAG conditions.

In the investigation of the application of RAM in the mechanochemical synthesis of halogen bonded cocrystals, eleven cocrystals were prepared, as outlined in Table 1. Specifically, cocrystal **1b** was prepared *via* RAM by introducing a 1 : 2 molar ratio of the donor to the acceptor into a 1-dram glass vial, and subjecting it to pressure waves of 80 g for a duration of 45 min. The resulting PXRD pattern, as illustrated in Fig. 2, confirms the successful formation of the RUYHID cocrystal (Table 1) using the pristine solvent-free resonance acoustic mixing approach. To validate the reproducibility and versatility of RAM in producing halogen-bonded cocrystals and to make a comparative assessment with conventional mechanochemistry methods, we employed ball milling under identical synthesis conditions for the preparation of cocrystal **1b**. Remarkably, the PXRD data indicate a striking similarity between the cocrystals obtained through

these two distinct methods, confirming the formation of a pure and stable phase of cocrystal **1b**.

Subsequently, cocrystal **2b** was synthesized using RAM, employing a 1 : 3 molar ratio of donor **2** to acceptor **b**, with an 80 g acceleration for a duration of 50 min. Additionally, a parallel synthesis was carried out using ball milling with a frequency of 30 kHz and a duration of 45 min. The PXRD patterns, depicted in Fig. 2 (and ESI†), provide compelling evidence for the formation of a pure and stable RUYJAX phase in both cases.

It should be noted that our optimization process for RAM synthesis commenced with neat powders to avoid the use of solvents. Additionally, we explored various preparation times, including 15, 30, and 45 min. The results presented herein encompass the optimized synthesis conditions for each cocrystal *via* both RAM and ball milling techniques. It was observed that the exclusion of liquid additives yielded pure cocrystals only in the case of **1a(ii)**, **1b**, and **2b**. This phenomenon can be attributed to the superior properties of acceptors TMP(**a**) and DMP(**b**), characterized by their enhanced nucleophilicity and reduced steric hindrance, facilitating efficient halogen bond formation. This distinction is expected to result in shorter bond lengths and stronger XB interactions within these compounds. This is evident in the geometric parameters obtained from SCXRD data where the R_{XB} values of 0.85, 0.76 and 0.78 were determined for the I···N interactions in **1a(ii)**, **1b**, and **2b** cocrystals, respectively.

To address this issue, we adopted a strategy involving the introduction of liquid additives[33] within the range of 0.05 to 0.7 μL per milligram of reactants ($\eta = 0.05$ to 0.7) in the reaction jar. In this context, the RAM of **1** and **c** reactants in a 1 : 2 molar ratio, supplemented with chloroform at an $\eta = 0.1$ μL mg^{-1} ratio, yielded the pure and stable cocrystal **1c** (refcode: JAQMIY). Similarly, the syntheses of cocrystals **1d** and **1e**, as confirmed by their PXRD patterns displayed in Fig. 2, were achieved by introducing equimolar quantities of starting materials, along with an $\eta = 0.5$ μL mg^{-1} of THF. Applying an 80 g acceleration for 50 min *via* RAM yielded the EXIFEX and EXIFAT phases for **1e** and **1d**, respectively. Comparison with the simulated PXRD pattern alongside those of the RAM and ball mill products unequivocally establishes the production of a pure phase of cocrystal **1e** through both mechanochemical methods.

To further investigate the influence of the type and quantity of liquid additives on RAM-synthesized XB cocrystals, a screening experiment was conducted on cocrystal **2c**. Samples were prepared under neat conditions, with 0.1 μL mg^{-1} $CHCl_3$, and with 0.1 μL mg^{-1} THF in the RAM process. Fig. 3 showcases the PXRD results, revealing incomplete conversion in the neat and $CHCl_3$ experiments while highlighting the formation of a pure SAJDEP phase when employing THF as the liquid additive in RAM cocrystallization for cocrystal **2c**. This comprehensive exploration of mechanochemical synthesis conditions and the influence of liquid additives underscores the versatility and effectiveness of RAM in the preparation of diverse halogen-bonded cocrystals, offering valuable insights into the optimization of this synthesis approach. Friščić and co-workers have

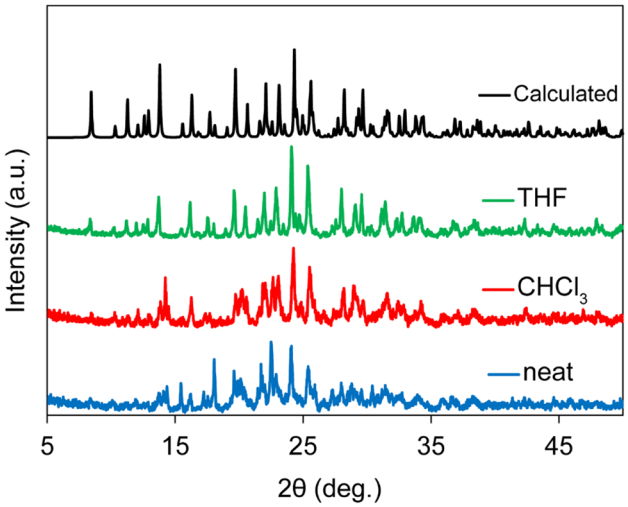

Fig. 3 Powder X-ray diffractograms for samples of **2c** produced using different RAM conditions: neat RAM (blue), 0.1 μL mg^{-1} $CHCl_3$ RAM (red), and 0.1 μL mg^{-1} THF RAM (green). The calculated PXRD pattern based on the SCXRD structure is shown in black.

discussed the optimization of the η value in liquid-assisted RAM applied to catalysis.[33]

In the preparation of cocrystals **2d** and **2e**, equimolar quantities of the starting materials were introduced into the reaction vessel, accompanied by the addition of 0.7 μL mg^{-1} of $CHCl_3$. The resulting PXRD patterns, as illustrated in Fig. 2, unequivocally demonstrate the successful formation of these novel cocrystals after a reaction duration of 50 min at 80 g acceleration. This is in excellent agreement with the simulated pattern derived using Mercury 4.2.0 software[65] based on newly acquired SCXRD data (*vide infra*). It is noteworthy that RAM proved to be an efficient and viable mechanochemical approach for the synthesis of these two novel XB cocrystals, eliminating the necessity for milling media and extensive mechanical grinding or abrasion processes.

During the RAM screening for cocrystal formation, with the compound **1a**, we observed intriguing results. Neat RAM for 45 min with a 1 : 2 ratio (donor : acceptor) led to the formation of the stable phase of the **1a(ii)** stoichiomorph (refcode: KIHRAX)[61] which was not achievable with other mechanochemical methods like ball milling. Addition of 85 μL of chloroform ($\eta = 0.2$ μL mg^{-1}) and mixing time of 50 min, however, transform the reactants (1 : 2 ratio (donor : acceptor)) instead to the **1a(i)** stoichiomorph (refcode = JAQMAQ),[60] the same product as obtained when ball milling for 45 min with same liquid additive. These results are presented in Fig. 4, showcasing PXRD patterns acquired for both neat and liquid-added RAM products. This finding affirms that varying RAM conditions can yield distinct stoichiomorphs of compound **1a** and highlights the remarkable potential of RAM as a tool for controlling and influencing stoichiomorphism and polymorphism. Notably, our attempts to prepare the **1a(ii)** stoichiomorph using ball milling were unsuccessful. It is important to mention that previous applications of mechanochemical ball milling, involving neat grinding and LAG, have resulted in the formation of different

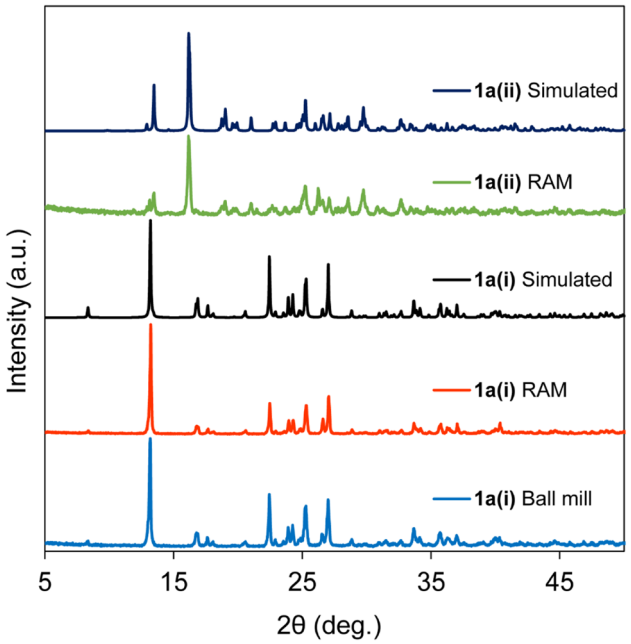

Fig. 4 X-ray diffractograms of **1a(i)** and **1a(ii)** cocrystalline powders prepared under ball milling and RAM conditions. See Table 1 and the main text for details. Simulated diffractograms are generated from the known single-crystal X-ray structures with refcodes JAQMAQ (**1a(i)**) and KIHRAX (**1a(ii)**).

polymorphs, as reported elsewhere.[66] To the best of our knowledge, the present work represents the first instance where the formation of different stable cocrystalline phases can be controlled using RAM; related work on controlling polymorphism with RAM has recently been reported.[33]

While the exact mechanism underlying this phenomenon remains incompletely understood, two distinct factors appear to influence the formation of different products *via* RAM. Firstly, in the liquid-assisted approach, the presence of a liquid component can enhance the reaction rate by introducing degrees of orientational and conformational freedom to the molecules at various interfaces.[67] Additionally, adding liquid may lead to the formation of a mobile surface layer at the molecule interface, which can enhance the reactivity of the reactants[68] and affect the resulting polymorphs. The second factor could be particularly apposite for RAM, which operates as a milder mechanochemical methodology where the reaction occurs through the direct impact of the reactant particles.

(ii) Single crystal X-ray diffraction

The crystal structures of **1a(i)** (CCDC 259702),[60] **1a(ii)** (CCDC 1854044),[61] **2a** (CCDC 1505893),[9] **1b** (CCDC 773127),[64] **2b** (CCDC 773130),[64] **1c** (CCDC 259705),[60] **2c** (CCDC 1505895),[9] **1d** (CCDC 824297),[63] and **1e** (CCDC 824296)[63] have been previously documented. In this study, we determined the single crystal X-ray diffraction (SCXRD) structures for compounds **2d** and **2e** to enhance our comprehension of halogen bonding interactions within these supramolecular assemblies.

SCXRD analysis revealed a 1 : 1 stoichiometry of *sym*-TFTIB to PheDON in **2d**. This compound crystallizes in a monoclinic crystal system, belonging to the $P2_1/c$ space group. The volume of the unit cell is determined to be 15 288(7) Å^3, and the crystal contains 32 molecules in the unit cell. The unit cell parameters and the other relevant information are presented in Table 2. As can be seen in Fig. 5(C), in **2d**, both nitrogen atoms of the bidentate PheDON interact with one of the *sym*-TFTIB iodine atoms, resulting in the observation of a slightly asymmetrical bifurcated halogen bond (XB) with I–N bond lengths of 2.997 and 3.297 Å (for example; there are 7 other pairs with similar distances as shown in Table 3). A straightforward layered packing arrangement is formed, where I–C and π—π interactions lead to a parallel stacking arrangement between *sym*-TFTIB and PheDON molecules as shown in Fig. 5(A), with intermolecular distances of 3.557 Å and 3.393 Å, respectively. Furthermore, the crystal structure reveals the presence of C–H···I and F···F interactions, which play a crucial role in extending the one-dimensional (1D) layer structures throughout the crystal network.

sym-TFTIB and DIZFON were cocrystallized to form the 1 : 1 cocrystal **2e** in the monoclinic space group $P2_1/c$. The supramolecular structure of **2e** is characterized by a monocoordinated XB of one *sym*-TFTIB with two acceptor moieties featuring one I–N and one I–O XB interaction (Fig. 5(D)). As is

Table 2 Crystallographic data and details

Compound	**2d**	**2e**
Chemical formula	$C_{18}H_6F_3I_3N_2O_2$	$C_{17}H_6F_3I_3N_2O$
CCDC number	2305189	2305188
FW (g mol^{-1})	719.95	691.94
Crystal colour	Orange	Yellow
Crystal system	Monoclinic	Monoclinic
Crystal space group	$P2_1/c$	$P2_1/c$
Temperature (K)	100 K	200 K
a, b, c (Å)	29.938(8), 18.399(5), 28.189(7)	8.3178(7), 30.472(2), 7.4150(5)
α, β, γ (deg)	90, 100.074(3), 90	90, 94.297(4), 90
V (Å^3)	15 288(7)	1874.1(2)
Z	32	4
R_1 (final)	0.1051	0.0504
wR_2 (final)	0.2484	0.0999

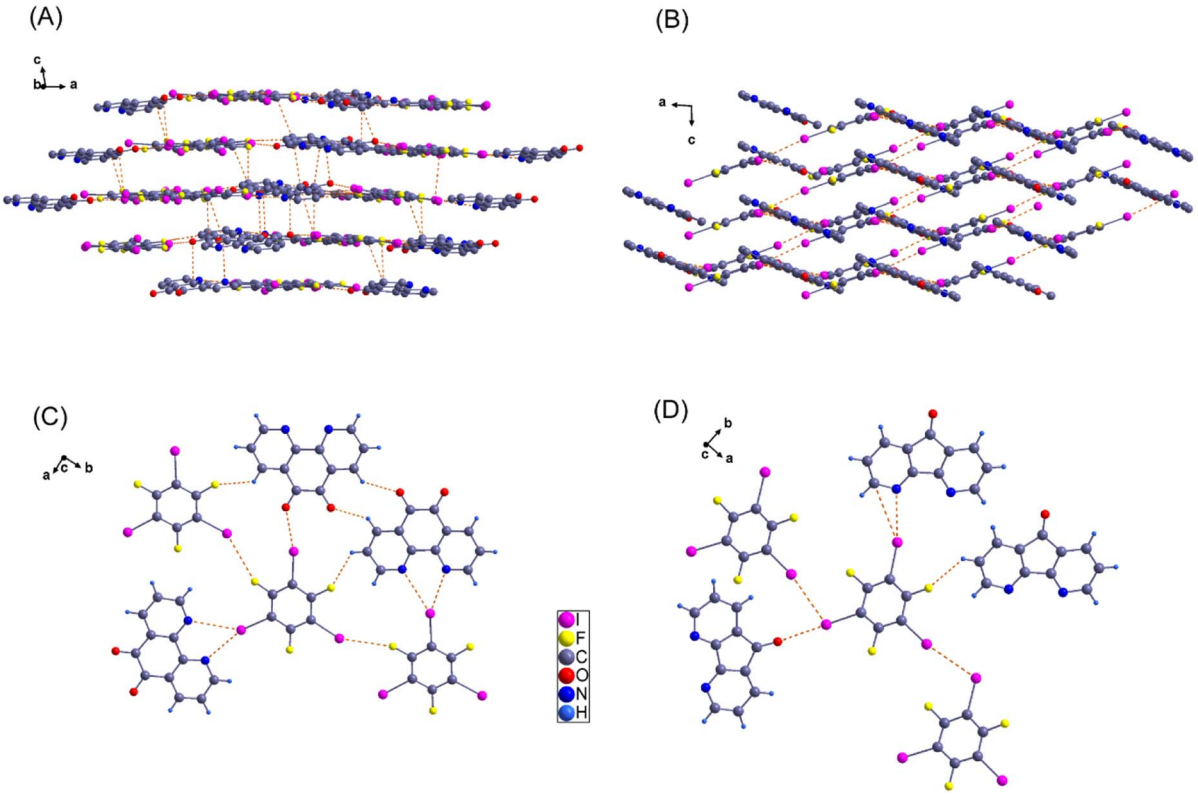

Fig. 5 Two novel crystal structures of compound **2d** (left, parts (A) and (C)) and **2e** (right, parts (B) and (D)) showing halogen bonds (dashed lines) in compounds **2d** and **2e**. In cocrystal **2d**, the iodine interacts with two nitrogen atoms making a bifurcated halogen bond and one oxygen with a monocoordinated interaction. In compound **2e**, the iodine of the donor interacts with two crystallographically distinct acceptor moieties.

Table 3 Selected halogen bond geometrical parameters, including contact distance, angle, and normalized contact distance ratio (R_{XB})

Cocrystal	$d_{I\cdots N}$ (Å)	$\theta_{C-N\cdots I}$	$R_{XB\ (I)}$	$d_{I\cdots O}$ (Å)	$\theta_{C-N\cdots O}$	$R_{XB\ (O)}$
1a(i) (*p*-DITFB)·(TMP)	3.067	177.15	0.869	—	—	—
1a(ii) (*p*-DITFB)·(TMP)	3.001	177.51	0.850	—	—	—
2a (*sym*-TFTIB)·(TMP)	2.991	178.90	0.847	—	—	—
	2.993	179.81	0.849			
1b (*p*-DITFB)·(DMAP)	2.677	179.25	0.756	—	—	—
2b (*sym*-TFTIB)·(DMAP)	2.766	176.15	0.784	—	—	—
	2.886	168.58	0.818			
1c (*p*-DITFB)·(*o*-Phe)	3.01	159.03	0.853	—	—	—
	3.274	149.76	0.927			
2c (*sym*-TFTIB)·(*o*-Phe)	3.02	175.68	0.856	—	—	—
	3.148	164.18	0.892			
1d (*p*-DITFB)·(PheDON)	3.149	154.93	0.892	3.214	155.14	0.918
2d (*sym*-TFTIB)·(PheDON)	3.297, 3.011, 3.215, 3.047, 3.225, 3.097, 2.997, 3.326, 3.316, 3.026, 3.406, 3.029, 3.039, 3.259, 3.094, 3.230	144.8, 165.1, 166.7, 143.3, 165.6, 143.9, 159.0, 149.5, 160.8, 149.0, 162.4, 146.5, 158.7, 149.9, 144.6, 164.1	0.934, 0.853, 0.911, 0.863, 0.914, 0.877, 0.849, 0.942, 0.939, 0.857, 0.965, 0.858, 0.861, 0.923, 0.876, 0.91	2.884[a]	177.52	0.824
1e (*p*-DITFB)·(DIZFON)	2.924	165.10	0.828	3.036	163.02	0.867
2e (*p*-DITFB)·(PheDON)	2.968	158.66	0.841	2.931	177.52	0.824

[a] For this compound, we avoid detailing the entire list of I···O XB interactions and instead provide one example in this table.

depicted in Fig. 5(B), the **2e** cocrystal structure propagates in zigzag chains where each 1D chain is packed on the next *via* I–I intermolecular interactions between donor moieties, generating a 2D layered structure.

It is not surprising that the structure of **2e** lacks a bifurcated XB, consistent with conclusions reached in the study by Ji *et al.* on similar acceptor moieties.[63] This finding can be attributed to the relatively greater distance between the two electron-rich

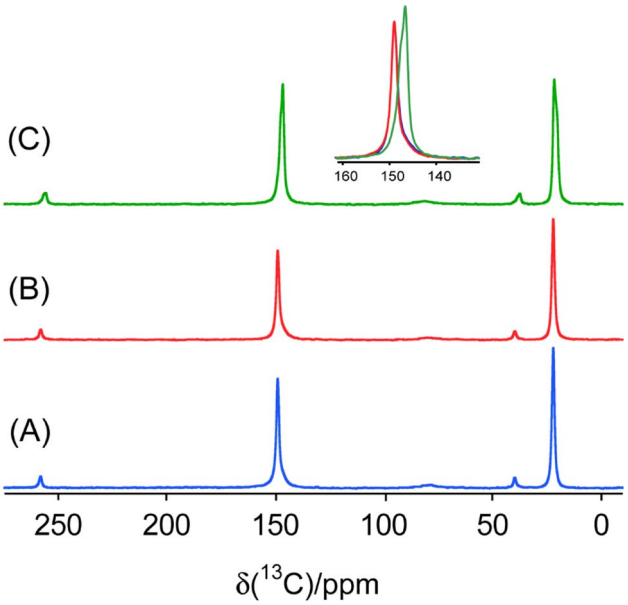

Fig. 6 $^{1}H \rightarrow {}^{13}C$ CP/MAS solid-state NMR spectra of sample **1a(i)** obtained by ball milling (blue, A), RAM (red, B), and the second stoichiomorph **1a(ii)** obtained by RAM (green, C). Inset: overlay of peak for the C covalently bonded to N in these three products to illustrate the identical ^{13}C chemical shifts for the ball milled and RAM products for **1a(i)**, but different chemical shift for the second stoichiomorph **1a(ii)**.

atoms (N) in DIZFON molecules, exceeding the threshold for the formation of a three-centered XB involving I and two N atoms. The distance between I and N in the XB interaction is measured at 2.968 Å, which is shorter than the corresponding bifurcated I–N XB in the **2d** cocrystal. This observation aligns with the concept that a monocoordinated XB is expected to be stronger than a bifurcated XB.[63]

(iii) Solid-state NMR spectroscopy

To further characterize the halogen-bonded cocrystals produced *via* RAM, we conducted ^{13}C CP/MAS SSNMR spectroscopy on all of the samples. The use of $^{1}H \rightarrow {}^{13}C$ cross-polarization has been demonstrated as a reliable and effective indirect method for characterizing the formation of XB cocrystals.[9] This technique allows us to gain insights into changes in the crystallographic and electronic environment surrounding the carbon atom covalently bonded to the nitrogen atom (C–N) in the acceptor moieties. The principle underlying this technique lies in the polarization transfer from protons to the carbon atom covalently bonded to the nitrogen atom. This ^{13}C nucleus is indirectly engaged in each XB (*i.e.*, one bond removed), and is subjected to small changes in electronic and crystallographic environment upon cocrystallization. Consequently, this involvement results in changes in the chemical shifts, exemplified in Fig. 6 for the two stoichiomorphs of **1a** (**1a(i)** and **1a(ii)**). The distinct ^{13}C chemical shifts observed for the two samples reflect differences in the local nuclear environment.

Fig. 7 and 8 depict the ^{13}C CP/MAS NMR spectra of XB acceptor moieties alongside all cocrystals formed with the two XB donors, **1** and **2**. Notable changes in chemical shifts are evident upon the formation of XB cocrystals, with their corresponding δ_{iso} values listed in Table 4. Strikingly, these NMR data also provide clear evidence that products generated *via* RAM and *via* ball milling are isomorphic; this is consistent with the PXRD data presented above and in the ESI.† In some cases, ball milling gives broader NMR lines which could be indicative of partial amorphization of the product (see ESI†). This effect

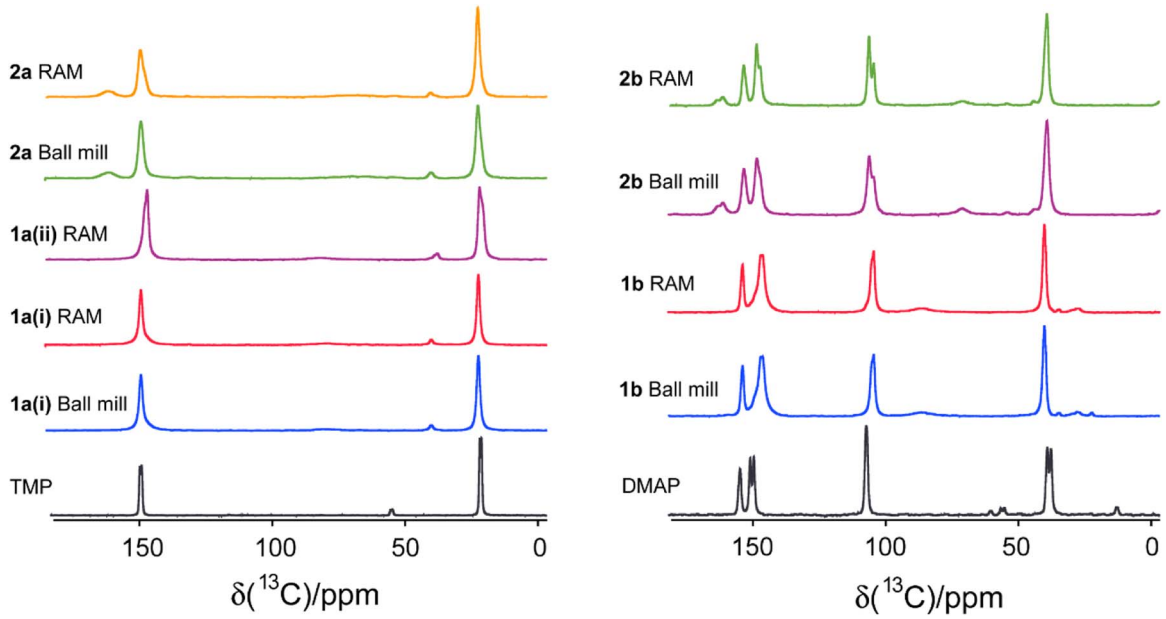

Fig. 7 Comparison of ^{13}C CP/MAS NMR spectra for monotopic XB acceptors (TMP and DMAP) and their respective cocrystals produced *via* ball milling and RAM. The corresponding chemical shifts are listed in Table 4.

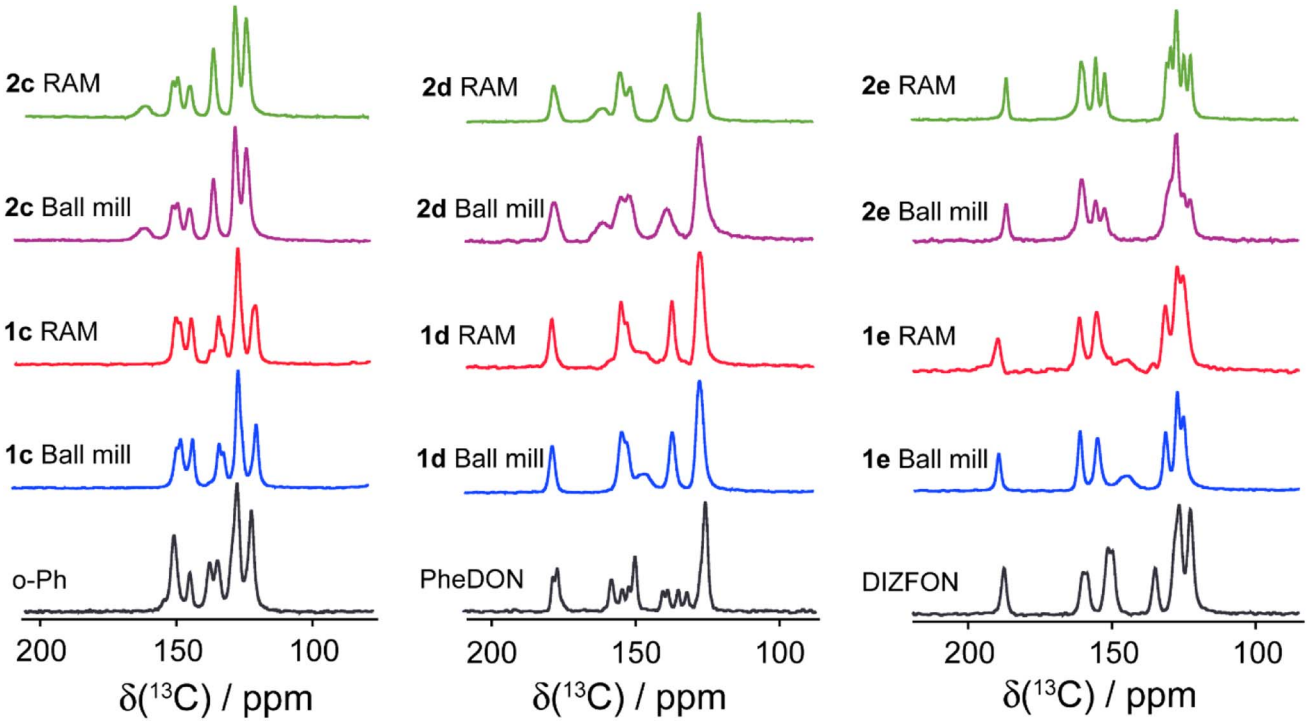

Fig. 8 Comparison of ^{13}C CP/MAS NMR spectra of ditopic XB acceptors (*o*-Ph, PheDON, and DIZFON) and their cocrystals produced *via* ball milling and RAM. The chemical shifts are detailed in Tables 4 and 5.

Table 4 Experimental ^{13}C chemical shifts of the carbon covalently bonded to the nitrogen in the XB acceptor moieties, based on ^{1}H → ^{13}C CP/MAS NMR experiments[a]

Cocrystal	XB acceptor	δ_{iso}/ppm XB acceptor	δ_{iso}/ppm cocrystal
1a(i)	TMP	142.7 & 149.1 ± 0.1	149.3 ± 0.3[b]
1a(ii)	TMP	142.7 & 149.1 ± 0.1	147.1 ± 0.5
2a	TMP	142.7 & 149.1 ± 0.1	149.5 ± 0.6
1b	DMAP	150.9 & 149.5 ± 0.1	146.6 ± 0.6
2b	DMAP	150.9 & 149.5 ± 0.1	147.8 ± 0.7
1c	*o*-Ph	150.8 & 145.1 ± 0.3	149.8 & 148.4 & 144.0 ± 0.3
2c	*o*-Ph	150.8 & 145.1 ± 0.3	151.2 & 149.5 & 145.1 ± 0.4
1d	PheDON	158.4 & 154.7 152.5 & 150.3 ± 0.4	154.8 & 153.2 & 147.1 ± 0.6
2d	PheDON	158.4 & 154.7 152.5 & 150.3 ± 0.4	161.4 & 155.5 & 152.0 ± 0.5
1e	DIZFON	160.7 & 152.0 ± 0.4	162.5 & 156.4 ± 0.4
2e	DIZFON	160.7 & 152.0 ± 0.4	162.1 & 157.1 & 154.0 ± 0.4

[a] Chemical shifts of donor molecules are also evident; these are marked on spectra shown in the ESI. [b] Errors in chemical shift measurements are attributed to the lack of certainty regarding the quantitative impact of residual ^{13}C–^{14}N dipolar coupling on peak positions.

could possibly be reduced by using shorter milling times, but these experiments were not pursued presently.

In a statistical and computational analysis conducted by Allen *et al.* on NO_2–X synthons involving both monocoordinate and bifurcated XB, it was observed that as the interaction distance decreased, the XB angles tended to become more directional and linear.[69] This observation suggests that bifurcated halogen bonding interactions, where one halogen atom interacts with two Lewis bases, will correlate with smaller C–X···O angles. Conversely, smaller angles correlate with weaker interactions when compared to more linear monocoordinated XB interactions. In the cocrystals involving acceptor molecules **c** and **d** with donors **1** and **2**, which engage in bifurcated halogen-bonded interactions, the contact lengths between I and N atoms are relatively long, corresponding to weaker XB interactions. Consequently, the C–N covalent bond in the acceptor molecule will be

Table 5 Experimental ^{13}C chemical shifts of the carbon covalently bonded to I and F in the XB donor moieties, based on ^{1}H → ^{13}C CP/MAS experiments

Cocrystal	XB donor	δ_{iso}/ppm C–I	δ_{iso}/ppm C–F
1a(i)	*p*-DITFB	78.7 ± 0.8	—
1a(ii)	*p*-DITFB	82.3 ± 0.8	—
2a	*sym*-TFTIB	68.6 ± 2.2	161.9 ± 0.9
1b	*p*-DITFB	86.7 ± 1.4	—
2b	*sym*-TFTIB	71.2 ± 0.9	163.4 ± 0.6
1c	*p*-DITFB	77.4 ± 1.4	—
2c	*sym*-TFTIB	67.1 ± 1.2	161.5 ± 0.8
1d	*p*-DITFB	73.8 ± 1.2	—
2d	*sym*-TFTIB	63.2 ± 1.4	161.6 ± 0.6
1e	*p*-DITFB	76.8 ± 1.2	—
2e	*sym*-TFTIB	68.6 ± 1.4	—[a]

[a] In **2e**, the resonance frequency of the C atom bonded to F is obscured by the intense and distinct signals from the acceptor moieties' carbon. Therefore, we are unable to report the chemical shift of the C–F carbon.

weakened less than it is in the presence of a stronger monocoordinated XB, resulting in a lower ^{13}C chemical shift for the C atom covalently bonded to the N atom within the acceptor moiety. More generally, the data in Table 4 show that the ^{13}C chemical shifts of the acceptor molecules can increase or decrease upon cocrystallization; increases are generally noted for TMP and DIZFON, while decreases are noted for DMAP and more subtle changes are noted for *o*-Ph and PheDON.

In another study conducted by our group,[70] it was shown that an increase in the C–I bond length of halogen bond donor **1** as a result of XB formation corresponded to an increase in the ^{13}C chemical shift. The δ_{iso} values for ^{13}C covalently bonded to iodine and fluorine in the XB donor moieties are listed in Table 5. Consistent with previous work, increases in the C–I chemical shifts relative to that for pure donor **1** (76.50(0.50) ppm)[70] and for pure donor **2** (67.6 ± 2.4 ppm)[9] are generally observed. Interestingly, exceptions are seen in both cases for cocrystals formed with acceptor **d**, which forms bifurcated halogen bonds; such exceptions could therefore possibly be NMR signatures of bifurcated XB, but more data are needed to confirm the generality of this finding.

Fluorine-19 SSNMR spectroscopy is a powerful technique that has found extensive utility in characterizing halogen-bonded compounds due to the high receptivity of fluorine nuclei, high natural abundance, and the wide chemical shift range.[9,71] Fig. 9 illustrates the ^{19}F MAS SSNMR spectra acquired for all cocrystals and the perfluorinated XB donor starting materials. Importantly, changes in the ^{19}F chemical shift upon the formation of halogen-bonded cocrystals serve as valuable independent indicators of cocrystallization events. These

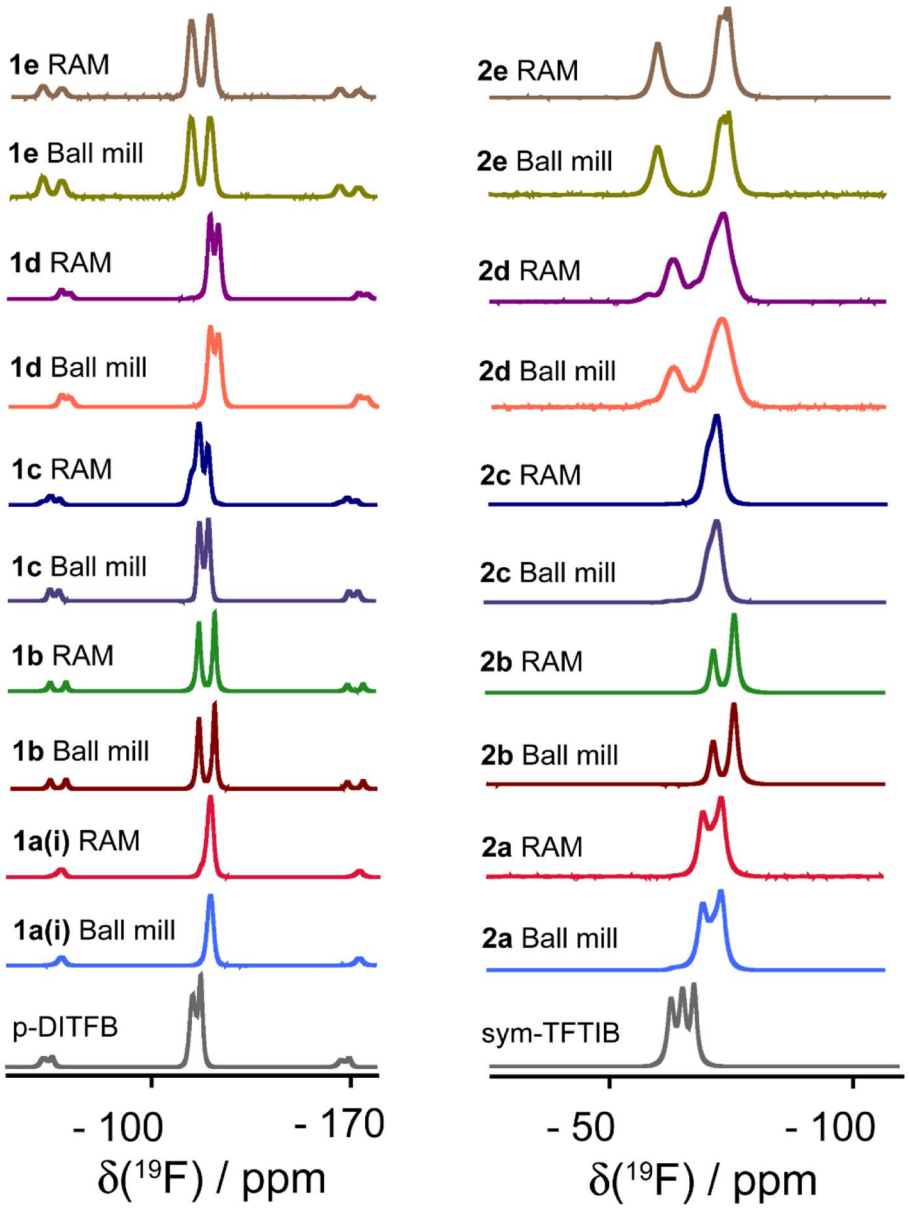

Fig. 9 Comparison of ^{19}F MAS SSNMR spectra of XB donors (*p*-DITFB and *sym*-TFTIB) and their cocrystals produced *via* ball milling and RAM. The chemical shifts are detailed in Table 6.

Table 6 Experimental ^{19}F chemical shifts of the halogen-bond donor moieties

Cocrystal	δ_{iso}/ppm cocrystal	XB donor	δ_{iso}/ppm XB donor
1a(i)	−118.9 ± 0.5	*p*-DITFB	−112.6 & −115.5 ± 0.6
1b	−114.8 & −120.4 ± 0.3		
1c	−115.0 & −118.3 ± 0.6		
1d	−118.8 & −121.7 ± 0.6		
1e	−121.2 & −118.8 ± 0.7		
2a	−68.3 & −72.1 ± 0.7	*sym*-TFTIB	−61.8 & −64.1 & −66.5 ± 0.3
2b	−70.4 & −74.8 ± 0.3		
2c	−71.2 ± 0.8		
2d	−62.2 & −72.6 ± 0.7		
2e	−59.1 & −72.0 & −73.4 ± 0.4		

spectra also provide an additional independent perspective that the products obtained *via* RAM and *via* ball milling are identical.

The ^{19}F chemical shifts are listed in Table 6, and the results demonstrate a consistent and notable decrease in the ^{19}F chemical shift for all samples upon the formation of halogen-bonded cocrystals. Since the crystallographic and electronic environment encountered by ^{19}F nuclei are highly sensitive to XB and certain short interactions involving ^{19}F nuclei with I or H atoms, as revealed by XRD, the extent of chemical shift changes exhibits variability across the compounds. Shifts on the order of up to −8 ppm are observed as a result of cocrystallization. These findings highlight the sensitivity of ^{19}F SSNMR as a probe to detect structural changes associated with XB cocrystallization. It is noted that while the ^{19}F NMR resonances for cocrystal **2d**, which features a large number of crystallographically non-equivalent molecules, are somewhat broader than for the other cocrystals, there is no clear spectral resolution of these multiple sites.

Conclusions

We have demonstrated that resonant acoustic mixing can consistently promote halogen-bond-induced cocrystallization of donor and acceptor molecules. Eleven halogen-bonded cocrystals have been prepared *via* RAM, including two novel structures which were characterized by single-crystal X-ray diffraction and one novel stoichiomorphic product which is inaccessible *via* ball milling. One of the notable advantages of RAM-based cocrystallization is its capacity to transform reactants into halogen-bonded interaction products through direct interactions, both under neat mixing conditions and when aided by the addition of small amounts of polar or moderately polar solvents. For most cocrystals studied herein, the inclusion of even a minimal quantity of these solvents serves to significantly enhance the cocrystallization process and increase the completeness of the transformation, further highlighting the potential of RAM in optimizing cocrystal synthesis. Powder X-ray diffraction and ^{13}C CP/MAS and ^{19}F MAS NMR spectroscopy have provided compelling evidence for the phase purity of samples obtained from RAM experiments and for the degree of polymorphic control available when small volumes of liquid are employed in mechanochemical reactions. Overall, this work demonstrates the potential of RAM for the production of known and novel cocrystalline assemblies, including polymorphic and stoichiomorphic structures.

Data availability

Data are available upon reasonable request from the authors.

Author contributions

A. N. prepared samples, carried out PXRD and SSNMR experiments, analysed all data, and wrote the first draft of the manuscript, and edited the manuscript. J. S. O. solved the single-crystal X-ray structures. D. L. B. directed research, secured funding, analysed data, and wrote and edited the manuscript.

Conflicts of interest

The authors declare they have no conflicts of interest.

Acknowledgements

D. L. B. is grateful to the Natural Sciences and Engineering Research Council of Canada for funding. The authors thank the solid-state NMR group at the University of Ottawa for helpful comments, and Dr Patrick Szell and Dr Tristan Georges for technical assistance.

References

1 P. Politzer, J. S. Murray and T. Clark, *Phys. Chem. Chem. Phys.*, 2010, **12**, 7748–7757.
2 L. C. Gilday, S. W. Robinson, T. A. Barendt, M. J. Langton, B. R. Mullaney and P. D. Beer, *Chem. Rev.*, 2015, **115**, 7118–7195.
3 A. Priimagi, G. Cavallo, P. Metrangolo and G. Resnati, *Acc. Chem. Res.*, 2013, **46**, 2686–2695.
4 A. Mukherjee, S. Tothadi and G. R. Desiraju, *Acc. Chem. Res.*, 2014, **47**, 2514–2524.
5 P. Auffinger, F. A. Hays, E. Westhof and P. S. Ho, *Proc. Natl. Acad. Sci. U. S. A.*, 2004, **101**, 16789–16794.
6 M. R. Scholfield, C. M. Vander Zanden, M. Carter and P. S. Ho, *Prot. Sci.*, 2013, **22**, 139–152.
7 T. Clark, M. Hennemann, J. S. Murray and P. Politzer, *J. Mol. Model.*, 2007, **13**, 291–296.
8 G. R. Desiraju, P. S. Ho, L. Kloo, A. C. Legon, R. Marquardt, P. Metrangolo, P. Politzer, G. Resnati and K. Rissanen, *Pure Appl. Chem.*, 2013, **85**, 1711–1713.
9 P. M. J. Szell, S. A. Gabriel, R. D. D. Gill, S. Y. H. Wan, B. Gabidullin and D. L. Bryce, *Acta Crystallogr., Sect. C: Struct. Chem.*, 2017, **73**, 157–167.
10 A. Bondi, *J. Phys. Chem.*, 1964, **68**, 441–451.
11 P. S. Ho, *Future Med. Chem.*, 2017, **9**, 637–640.

12 R. Wilcken, M. O. Zimmermann, A. Lange, A. C. Joerger and F. M. Boeckler, *J. Med. Chem.*, 2013, **56**, 1363–1388.
13 P. Molina, F. Zapata and A. Caballero, *Chem. Rev.*, 2017, **117**, 9907–9972.
14 A. Ravi, A. S. Oshchepkov, K. E. German, G. A. Kirakosyan, A. V. Safonov, V. N. Khrustalev and E. A. Kataev, *Chem. Commun.*, 2018, **54**, 4826–4829.
15 L. Catalano, S. Perez-Estrada, H.-H. Wang, A. J.-L. Ayitou, S. I. Khan, G. Terraneo, P. Metrangolo, S. Brown and M. A. Garcia-Garibay, *J. Am. Chem. Soc.*, 2017, **139**, 843–848.
16 J.-P. Gliese, S. H. Jungbauer and S. M. Huber, *Chem. Commun.*, 2017, **53**, 12052–12055.
17 L. Carreras, M. Serrano-Torné, P. W. N. M. van Leeuwen and A. Vidal-Ferran, *Chem. Sci.*, 2018, **9**, 3644–3648.
18 S. L. James, C. J. Adams, C. Bolm, D. Braga, P. Collier, T. Friščić, F. Grepioni, K. D. M. Harris, G. Hyett, W. Jones, A. Krebs, J. Mack, L. Maini, A. G. Orpen, I. P. Parkin, W. C. Shearouse, J. W. Steed and D. C. Waddell, *Chem. Soc. Rev.*, 2012, **41**, 413–447.
19 K. Horie, M. Barón, R. B. Fox, J. He, M. Hess, J. Kahovec, T. Kitayama, P. Kubisa, E. Maréchal, W. Mormann, R. F. T. Stepto, D. Tabak, J. Vohlídal, E. S. Wilks and W. J. Work, *Pure Appl. Chem.*, 2004, **76**, 889–906.
20 L. Takacs, *JOM*, 2000, **52**, 12–13.
21 L. Takacs, *J. Therm. Anal. Calorim.*, 2007, **90**, 81–84.
22 L. Takacs, *J. Mater. Sci.*, 2004, **39**, 4987–4993.
23 *Ball Milling towards Green Synthesis: Applications, Projects, Challenges*, ed. A. Stolle and B. Ranu, Royal Society of Chemistry, Cambridge, UK, RSC Green Chemistry Series, No. 31, 2015, p. 303.
24 I. Huskić, C. B. Lennox and T. Friščić, *Green Chem.*, 2020, **22**, 5881–5901.
25 M. Solares-Briones, G. Coyote-Dotor, J. C. Páez-Franco, M. R. Zermeño-Ortega, C. M. de la O Contreras, D. Canseco-González, A. Avila-Sorrosa, D. Morales-Morales and J. M. Germán-Acacio, *Pharmaceutics*, 2021, **13**, 790.
26 D. E. Crawford, A. Porcheddu, A. S. McCalmont, F. Delogu, S. L. James and E. Colacino, *ACS Sustain. Chem. Eng.*, 2020, **8**, 12230–12238.
27 P. Cerreia Vioglio, M. R. Chierotti and R. Gobetto, *Adv. Drug Delivery Rev.*, 2017, **117**, 86–110.
28 D. Braga and F. Grepioni, *Angew. Chem., Int. Ed.*, 2004, **43**, 4002–4011.
29 T. Stolar, A. Prašnikar, V. Martinez, B. Karadeniz, A. Bjelić, G. Mali, T. Friščić, B. Likozar and K. Užarević, *ACS Appl. Mater. Interfaces*, 2021, **13**, 3070–3077.
30 L. Gonnet, C. B. Lennox, J.-L. Do, I. Malvestiti, S. G. Koenig, K. Nagapudi and T. Friščić, *Angew. Chem., Int. Ed.*, 2022, **61**, e202115030.
31 F. Effaty, L. Gonnet, S. G. Koenig, K. Nagapudi, X. Ottenwaelder and T. Friščić, *Chem. Commun.*, 2023, **59**, 1010–1013.
32 C. B. Lennox, T. H. Borchers, L. Gonnet, C. J. Barrett, S. G. Koenig, K. Nagapudi and T. Friščić, *Chem. Sci.*, 2023, **14**, 7475–7481.
33 L. Gonnet, T. H. Borchers, C. B. Lennox, J. Vainauskas, Y. Teoh, H. M. Titi, C. J. Barrett, S. G. Koenig, K. Nagapudi and T. Friščić, *Faraday Discuss.*, 2023, **241**, 128–149.
34 A. Pichon, A. Lazuen-Garay and S. L. James, *CrystEngComm*, 2006, **8**, 211–214.
35 K. Kubota, Y. Pang, A. Miura and H. Ito, *Science*, 2019, **366**, 1500–1504.
36 F. Toda, K. Tanaka and A. Sekikawa, *J. Chem. Soc., Chem. Commun.*, 1987, 279–280.
37 G. Kaupp, in *Organic Solid State Reactions*, ed. F. Toda, Springer Berlin Heidelberg, Berlin, Heidelberg, 2005, pp. 95–183.
38 K. Tanaka and F. Toda, *Chem. Rev.*, 2000, **100**, 1025–1074.
39 G. Kaupp, in *Encyclopedia of Physical Organic Chemistry*, John Wiley & Sons, Inc., 2017, pp. 1–80.
40 A. V. Trask, N. Shan, W. D. S. Motherwell, W. Jones, S. Feng, R. B. H. Tan and K. J. Carpenter, *Chem. Commun.*, 2005, 880–882.
41 T. Friščić, S. L. Childs, S. A. A. Rizvi and W. Jones, *CrystEngComm*, 2009, **11**, 418–426.
42 A. V. Trask, W. D. S. Motherwell and W. Jones, *Chem. Commun.*, 2004, 890–891.
43 A. O. Patil, D. Y. Curtin and I. C. Paul, *J. Am. Chem. Soc.*, 1984, **106**, 348–353.
44 M. C. Etter, Z. Urbanczyk-Lipkowska, M. Zia-Ebrahimi and T. W. Panunto, *J. Am. Chem. Soc.*, 1990, **112**, 8415–8426.
45 M. C. Etter and D. A. Adsmond, *J. Chem. Soc., Chem. Commun.*, 1990, 589–591.
46 V. R. Pedireddi, W. Jones, A. P. Chorlton and R. Docherty, *Chem. Commun.*, 1996, 987–988.
47 K. Lisac, S. Cepić, M. Herak and D. Cinčić, *Chem.: Methods*, 2022, **2**, e202100088.
48 X. Ding, A. W. Crawford, W. P. Derrick, D. K. Unruh, R. H. Groeneman and K. M. Hutchins, *Chem.–Eur. J.*, 2021, **27**, 16329–16333.
49 C. Schumacher, K.-N. Truong, J. S. Ward, R. Puttreddy, A. Rajala, E. Lassila, C. Bolm and K. Rissanen, *Org. Chem. Front.*, 2024, DOI: **10.1039/D3QO01512B**.
50 D. Braga, G. Palladino, M. Polito, K. Rubini, F. Grepioni, M. R. Chierotti and R. Gobetto, *Chem.–Eur. J.*, 2008, **14**, 10149–10159.
51 A. Pichon and S. L. James, *CrystEngComm*, 2008, **10**, 1839–1847.
52 H. M. Titi, J.-L. Do, A. J. Howarth, K. Nagapudi and T. Friščić, *Chem. Sci.*, 2020, **11**, 7578–7584.
53 D. J. am Ende, S. R. Anderson and J. S. Salan, *Org. Process Res. Dev.*, 2014, **18**, 331–341.
54 K. Nagapudi, E. Y. Umanzor and C. Masui, *Int. J. Pharm.*, 2017, **521**, 337–345.
55 R. Tanaka, S. Osotprasit, J. Peerapattana, K. Ashizawa, Y. Hattori and M. Otsuka, *Pharmaceutics*, 2021, **13**, 56.
56 M. Bui, P. Chakravarty and K. Nagapudi, *Faraday Discuss.*, 2022, **241**, 357–366.
57 S. R. Anderson, P. Dubé, M. Krawiec, J. S. Salan, D. J. am Ende and P. Samuels, *Propellants, Explos., Pyrotech.*, 2016, **41**, 783–788.

58 S. R. Anderson, D. J. am Ende, J. S. Salan and P. Samuels, *Propellants, Explos., Pyrotech.*, 2014, **39**, 637–640.
59 M. Michalczyk, W. Zierkiewicz and S. Scheiner, *Cryst. Growth Des.*, 2022, **22**, 6521–6530.
60 J. L. Syssa-Magale, K. Boubekeur, P. Palvadeau, A. Meerschaut and B. Schöllhorn, *CrystEngComm*, 2005, **7**, 302–308.
61 P. M. J. Szell, S. A. Gabriel, E. Caron-Poulin, O. Jeannin, M. Fourmigué and D. L. Bryce, *Cryst. Growth Des.*, 2018, **18**, 6227–6238.
62 R. Wang, D. Hartnick and U. Englert, *Z. Kristallogr.*, 2018, **233**, 733–744.
63 B. Ji, W. Wang, D. Deng and Y. Zhang, *Cryst. Growth Des.*, 2011, **11**, 3622–3628.
64 L. C. Roper, C. Präsang, V. N. Kozhevnikov, A. C. Whitwood, P. B. Karadakov and D. W. Bruce, *Cryst. Growth Des.*, 2010, **10**, 3710–3720.
65 C. F. Macrae, I. Sovago, S. J. Cottrell, P. T. A. Galek, P. McCabe, E. Pidcock, M. Platings, G. P. Shields, J. S. Stevens, M. Towler and P. A. Wood, *J. Appl. Crystallogr.*, 2020, **53**, 226–235.
66 A. V. Trask, W. D. S. Motherwell and W. Jones, *Cryst. Growth Des.*, 2005, **5**, 1013–1021.
67 N. Shan, F. Toda and W. Jones, *Chem. Commun.*, 2002, 2372–2373.
68 J.-L. Do and T. Friščić, *ACS Cent. Sci.*, 2017, **3**, 13–19.
69 F. H. Allen, J. P. M. Lommerse, V. J. Hoy, J. A. K. Howard and G. R. Desiraju, *Acta Crystallogr., Sect. B: Struct. Sci.*, 1997, **53**, 1006–1016.
70 J. Viger-Gravel, S. Leclerc, I. Korobkov and D. L. Bryce, *CrystEngComm*, 2013, **15**, 3168–3177.
71 C. M. Widdifield, G. Cavallo, G. A. Facey, T. Pilati, J. Lin, P. Metrangolo, G. Resnati and D. L. Bryce, *Chem.–Eur. J.*, 2013, **19**, 11949–11962.